

## Supplementary information

### Understanding the formation chemistry of native solid electrolyte interphase over Lithium anode and its implications using LiTFSI/TME-TTE electrolyte and polysulfide additive

Bikila Nagasa Olana,<sup>a, †</sup> Shih-Huang Pan,<sup>a, †</sup> Bing-Joe Hwang,<sup>a, b, c</sup> Holger Althues,<sup>d</sup> Jyh-Chiang Jiang,<sup>a, \*</sup> and Shawn D. Lin<sup>a, \*</sup>

<sup>a</sup>Department of Chemical Engineering, National Taiwan University of Science and Technology, Taipei 10617, Taiwan

<sup>b</sup>National Synchrotron Radiation Research Center (NSRRC), Hsinchu, 30076, Taiwan

<sup>c</sup>Sustainable Energy Development Center, National Taiwan University of Science and Technology, Taipei 10617, Taiwan

<sup>d</sup> Fraunhofer-Institute for Material and Beam Technology IWS, Winterbergstraße 28, 01277 Dresden, Germany

<sup>†</sup>B-N. Olana and S-H. Pan contributed equally to this work

\* Corresponding author's e-mail address: [sdlin@mail.ntust.edu.tw](mailto:sdlin@mail.ntust.edu.tw)

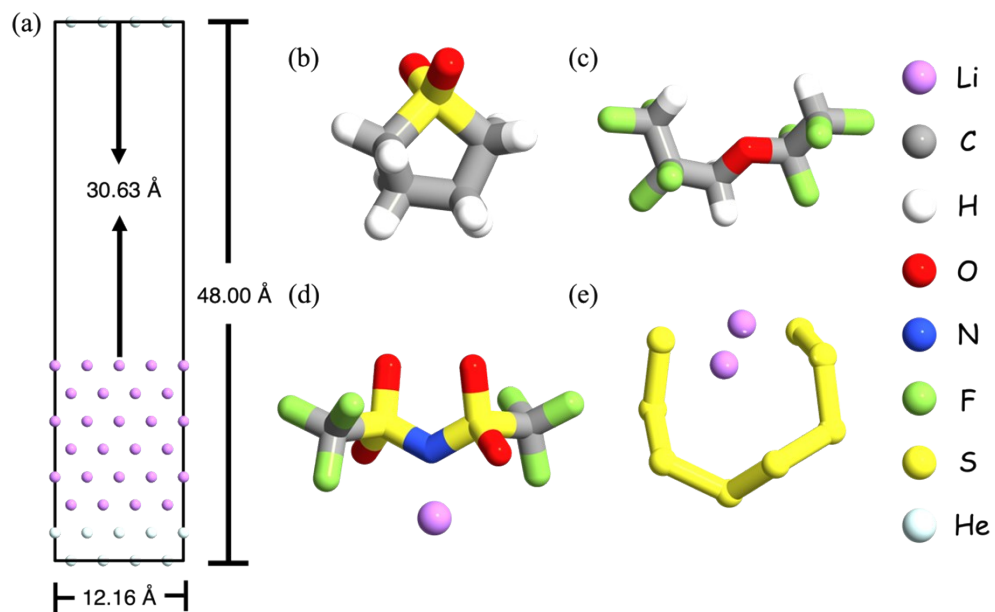


**Figure S1.** (a) The optimized Li (110) surface slab used in the AIMD simulations. Optimized electrolyte structures of (b) Tetramethylene sulfone (TMS) (c) 1,1,2,2-Tetrafluoroethyl 2,2,3,3-tetrafluoropropyl ether (TTE) (d) Lithium bis(trifluoromethanesulfonyl)imide (LiTFSI) (e) Lithium polysulfide (PS) at the CAM-B3LYP/6-311++G (d,p) level of theory. Color scheme: Li, purple; C, gray-black; H, white; O, red; N, blue; F, light green; S, yellow; He, gray-blue.

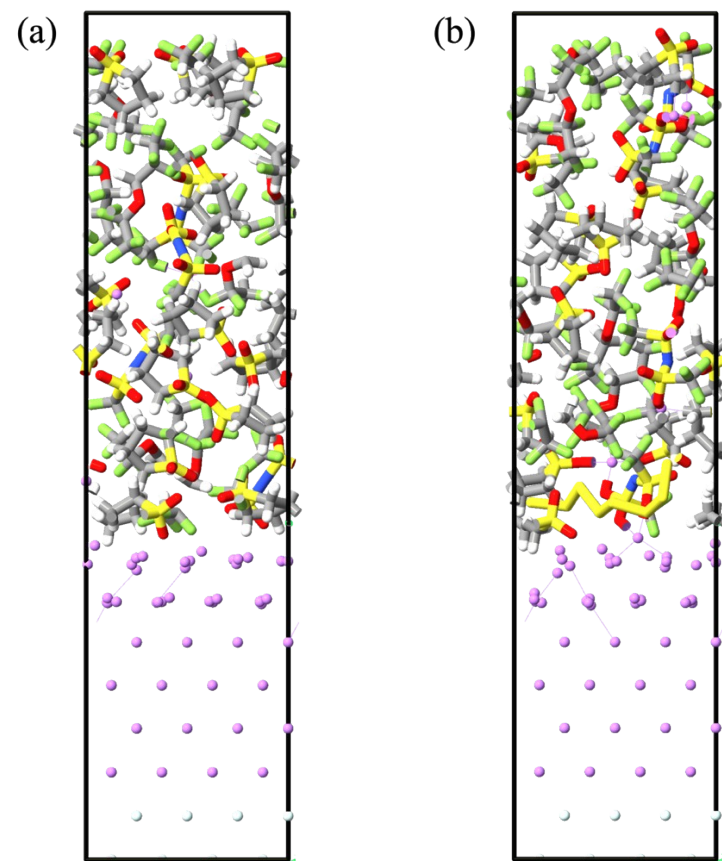


**Figure S2.** The constructed AIMD simulation boxes of LiTT (a) and LiTT-PS (b) electrolyte formulations.

**Table S1** FTIR spectra of liquid TMS, TTE, LiTT, and In Situ DRIFTS spectra over Li electrode at OCV.

Assignment	Liquid sample (FTIR)			Over Li (in-situ DRIFTS)			References
	TMS	TTE	LiTT	TMS	TTE	LiTT	
vas C-H	3009, 2952	3000	3010	2987	2995	2996	3004 <sup>1,2</sup> ,3037 <sup>3</sup> ,2950 <sup>4</sup>
vs C-H	2883	2906	2886	2882			2880 <sup>1,2</sup> , 2900 <sup>4</sup>
$\omega$ C-H	1450, 1415	1461,1415, 1407	1452,1418	1449,1414	1437	1463,1407, 1419	1448 <sup>1</sup> , 1412 <sup>1</sup> , 1445 <sup>4</sup>
vas O=S=O	1297		1354, 1297	1289		1351/21	1301 <sup>1</sup> , 1354 <sup>5,6</sup> , 1348 <sup>7</sup>
$\tau$ CH <sub>2</sub> + $\pi$ C-H	1311,1257, 1109	1361,1355	1257, 995	1253,1204, 1099	1319,1287	1288,1252	1109 <sup>2</sup> , 1362 <sup>3</sup> , 1248 <sup>8</sup>
vas C-F		1220,1192	1196		1220,1185	1196	1192 <sup>9,10</sup> , 1194 <sup>11</sup>
vs O=S=O	1147		1196,1147	1137		1196,1143	1147 <sup>1</sup> , 1139 <sup>5</sup> , 1143 <sup>12</sup>
vs C-F		1139	1147		1144	1143	1135 <sup>4</sup> , 1227 <sup>7</sup>
vas C-O-C/C-O		1122	1109		1124	1124	1140 <sup>9</sup> , 1180-1025 <sup>3</sup>
vas S-N-S			1059			1063	1060 <sup>6,11</sup> , 1065 <sup>5</sup> , 1051 <sup>5</sup>
$\nu$ C-C	1032	1023	1032		970	1032	1032 <sup>1,2</sup>
$\rho$ C-H	992, 906	968	995, 908	1032,988, 903		942	987 <sup>1</sup> , 903 <sup>1,2</sup>
vs C-O-C/C-O		835	835		847	839	816 <sup>9</sup> , 805 <sup>4</sup>
$\nu$ C-S (LiTFSI)			792			781	778 <sup>6</sup> , 790 <sup>5</sup>
vs S-N-S			763			758	761 <sup>6</sup> , 762 <sup>5</sup>
$\delta$ C-F/ $\nu$ C-S(TMS)	735	780	739	724	770	743	733 <sup>1,2</sup> , 739 <sup>6</sup> , 740 <sup>5</sup>
$\delta$ S-N-S			673,655			687, 674	655 <sup>5,6</sup>

vas: asymmetrical stretch, vs: symmetrical stretch,  $\nu$ : stretching,  $\delta$ : bending,  $\pi$ : wagging,  $\tau$ : twisting,  $\rho$ : rocking,  $\omega$ : scissoring

Figure S3 shows the FTIR spectra of liquid LiTFSI/TMS-TTE (LiTT) electrolytes and their components. The FTIR vibration bands of liquid TMS, TTE, and LiTFSI band assignments are presented in Table 1, consistent with previous reports.<sup>1-6,9</sup> The FTIR spectrum of TTE in Figure S3 (a) showed a main contributing band at 1122  $\text{cm}^{-1}$  and a shoulder at high wavenumber side that can be attributed to asymmetrical stretching of C-O-C ( $\nu_{as}$  C-O-C) and symmetrical stretching of C-F ( $\nu_s$  C-F) of fluoride ether, respectively, with corresponding  $\nu_{as}$  C-F,  $\nu_s$  C-O-C and  $\delta$  C-F (bending mode) at 1192, 835, and 780  $\text{cm}^{-1}$ .<sup>3,9</sup> The C-H vibration modes can be found at 3000 ( $\nu_{as}$  C-H), 2906 ( $\nu_s$  C-H), and 1407  $\text{cm}^{-1}$  ( $\omega$  C-H). TMS in Figure S3 (b) showed prominent bands from asymmetrical and symmetrical stretching of O=S=O at 1297 ( $\nu_{as}$  O=S=O) and 1147  $\text{cm}^{-1}$  ( $\nu_s$  O=S=O),<sup>2</sup> with corresponding C-H modes at 2952 ( $\nu_{as}$  C-H), 2883 ( $\nu_s$  C-H), 1415 ( $\omega$  C-H), 1257 ( $\pi$  C-H), 1109 ( $\tau$  C-H) and 906  $\text{cm}^{-1}$  ( $\rho$  C-H).<sup>1</sup> The absorbance band at 735  $\text{cm}^{-1}$  is attributed to the stretching vibration of S-C from the TMS ring. Surprisingly, the TMS-TTE mixture (Figure S3 (c), TMS: TTE = 1:1 (V:V)) showed nearly the same features as that of TMS, indicating the TMS signals dominate over that of TTE.

LiTT (LiTFSI/TTE-TMS) electrolyte (Figure S3 (d)) showed additional bands that can be assigned to LiTFSI at 1354 ( $\nu_{as}$  O=S=O), 1196 ( $\nu_s$  O=S=O/ $\nu_{as}$  C-F), 1059 ( $\nu_{as}$  S-N-S) and 763 ( $\nu_s$  S-N-S)  $\text{cm}^{-1}$ .<sup>5, 13</sup> Vibration bands of O=S=O and C-S from LiTFSI and TMS were found at different frequencies because of the different chemical bonding environments of O=S=O in LiTFSI and TMS. We assign  $\nu_s$  O=S=O from LiTFSI at 1196  $\text{cm}^{-1}$ <sup>5, 6, 12</sup> and that from TMS at 1147  $\text{cm}^{-1}$  with their corresponding  $\nu_{as}$  O=S=O at 1354 and 1297  $\text{cm}^{-1}$ , respectively. The C-S band of LiTFSI was found at 792  $\text{cm}^{-1}$  compared to that from TMS at 735  $\text{cm}^{-1}$ . The broad band at around 1200  $\text{cm}^{-1}$  can be due to the overlapping of  $\nu_s$  O=S=O and  $\nu_{as}$  C-F and the possible TMS interaction with LiTFSI may contribute to the band broadness.<sup>14</sup> When the PS was included as an additive of LiTT (Figure S3 (e)), no new absorbance band was observed, but the relative band intensities of LiTT-PS were different compared to that of LiTT, indicating the interaction between  $\text{Li}_2\text{S}_8$  and the other electrolyte components.

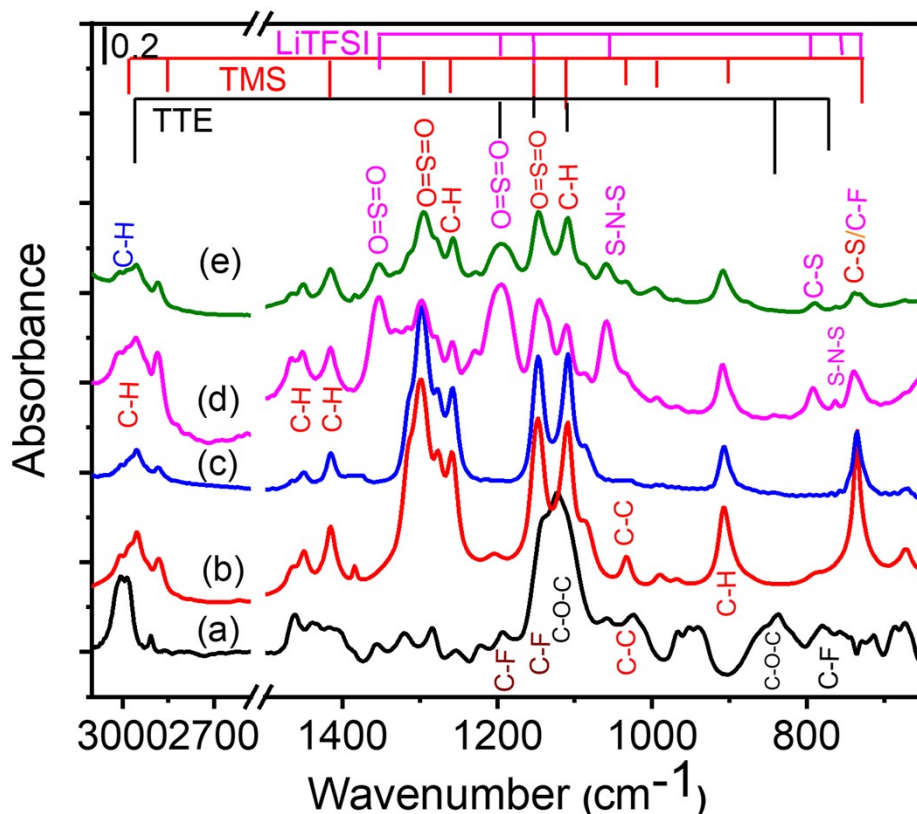


**Figure S3.** FTIR absorbance spectrum of liquid samples: (a) TTE, (b) TMS, (c) TMS: TTE = 1:1, (d) LiTT, and (e) LiTT-PS.

Figure S4 shows the different spectra of (LiTT-TMS-TTE) and (LiTT-PS-TMS-TTE). Figure S4 (a) (LiTT-TMS-TTE) shows bands at 1354 ( $\nu_{as}$  O=S=O), 1194 ( $\nu_s$  O=S=O/ $\nu_{as}$  C-F), 1135 ( $\nu_s$  C-F), 1059 ( $\nu_{as}$  S-N-S), 789 ( $\nu_s$  C-S/ S-N-S) and 745  $\text{cm}^{-1}$  ( $\delta$  C-F) attributed to LiTFSI as discussed above. When comparing the difference spectra of (LiTT-PS-TMS-TTE) (Figure S4 (b)) to that of (LiTT-TMS-TTE) (Figure S4 (a)), the presence of PS resulted in broadened bands (of O=S=O, S-N-S, and C-S) and their relative band intensity was changed. This suggests the presence of interaction between  $\text{Li}_2\text{S}_8$  with LiTFSI or TMS.

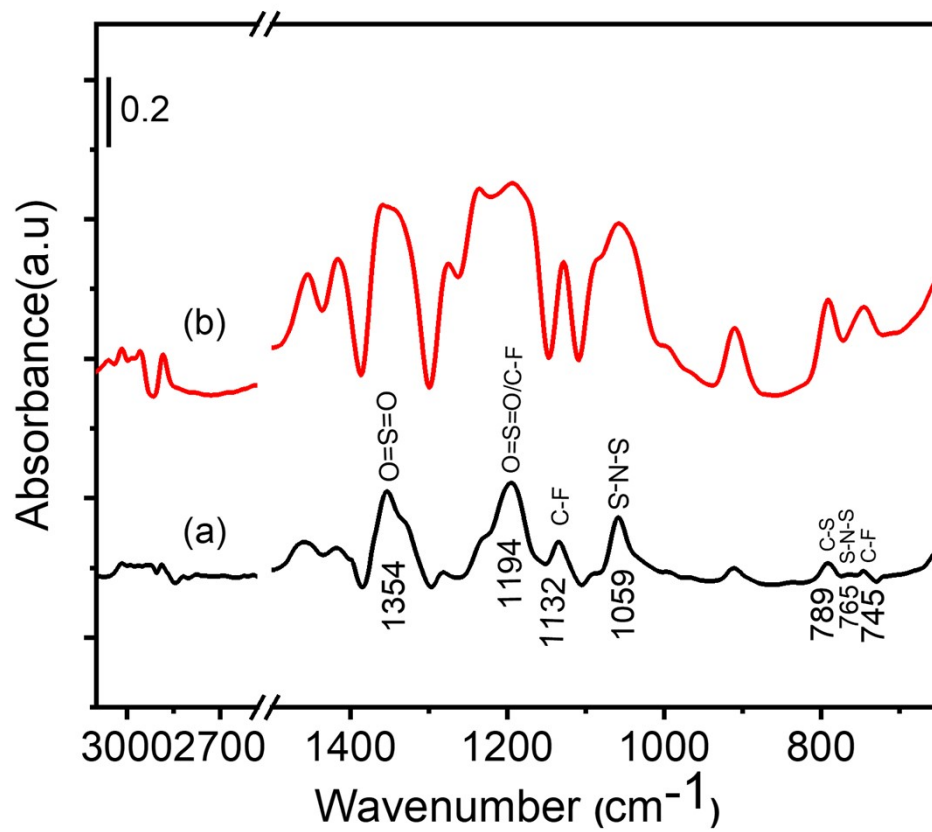


**Figure S4.** Difference spectra of FTIR spectra of liquid samples: (a) LiTT-TMS-TTE and (b) LiTT-PS-TMS-TTE.

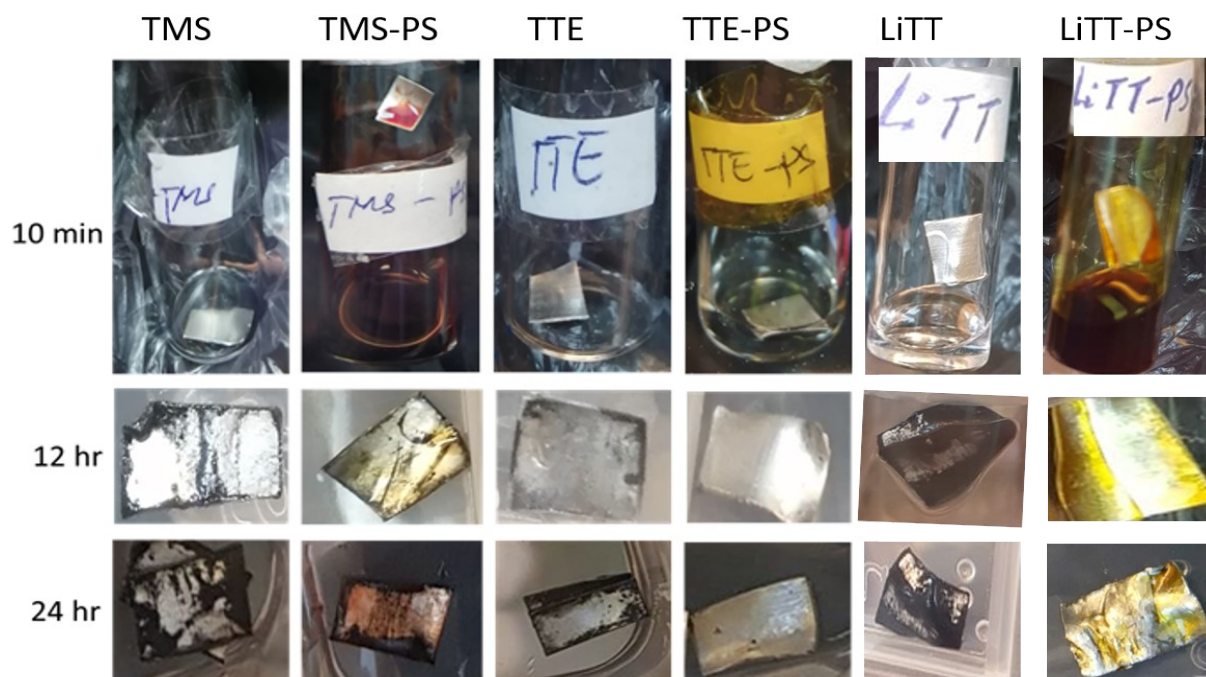


**Figure S5.** Images of Li foils immersed in TMS, TMS-PS, TTE, and TTE-PS, LiTT, and LiTT-PS after 10 minutes, 12 hours, and 24 hours, respectively. The experiments were performed inside an Ar-filled glove box.



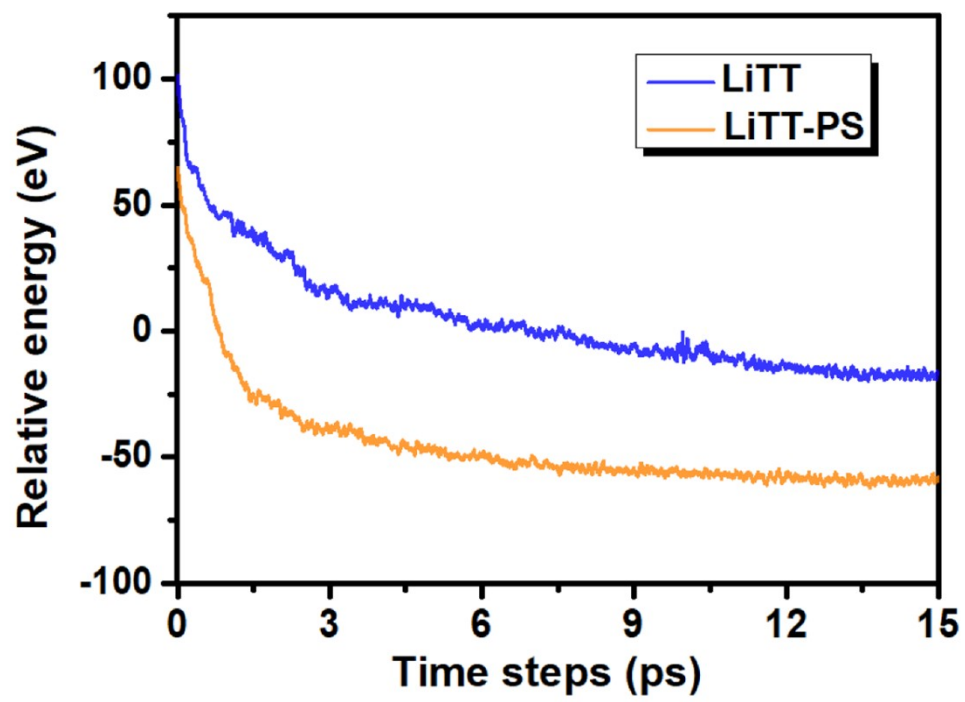
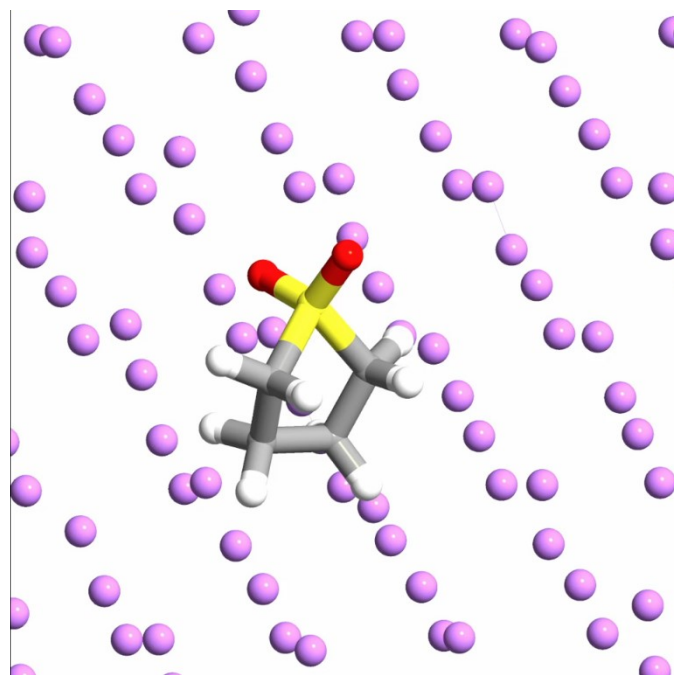


**Figure S6.** The relative energy fluctuations of the LiTT (blue line) and the LiTT-PS (orange line) systems over the AIMD simulation.




Video S1.mp4

**Video S1.** Molecular dynamic film of the decomposed TMS solvent adhered to the Li anode surface in the LiTT electrolyte formulation.

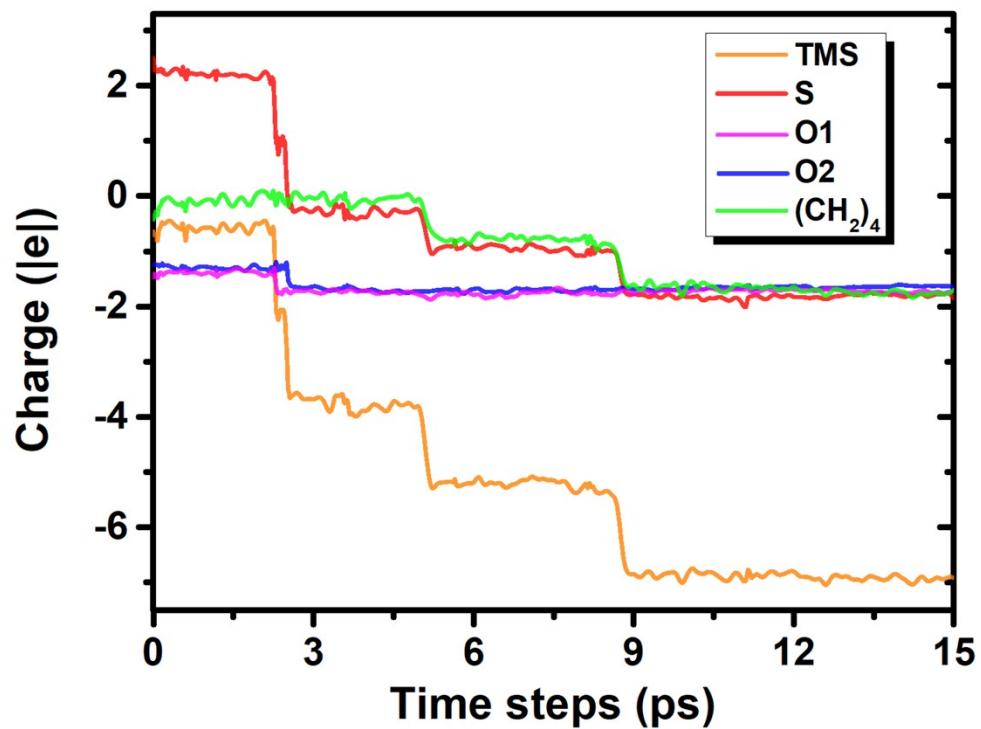
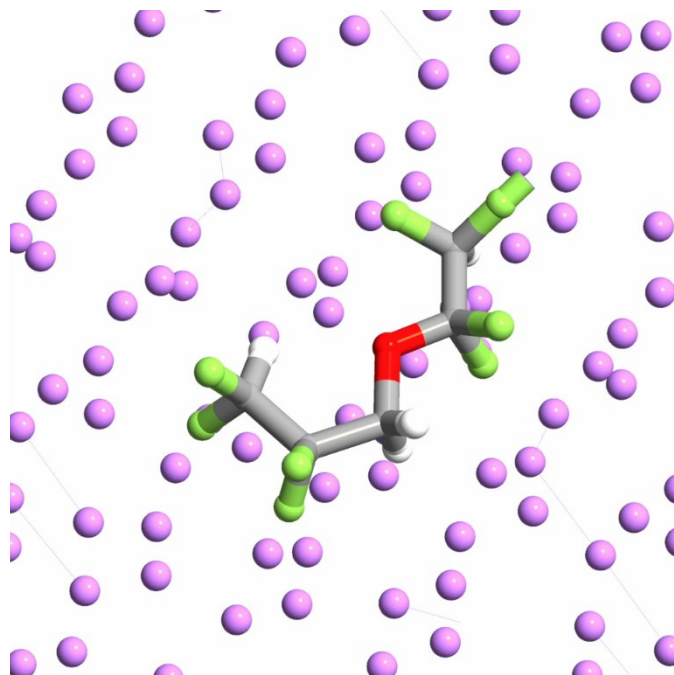
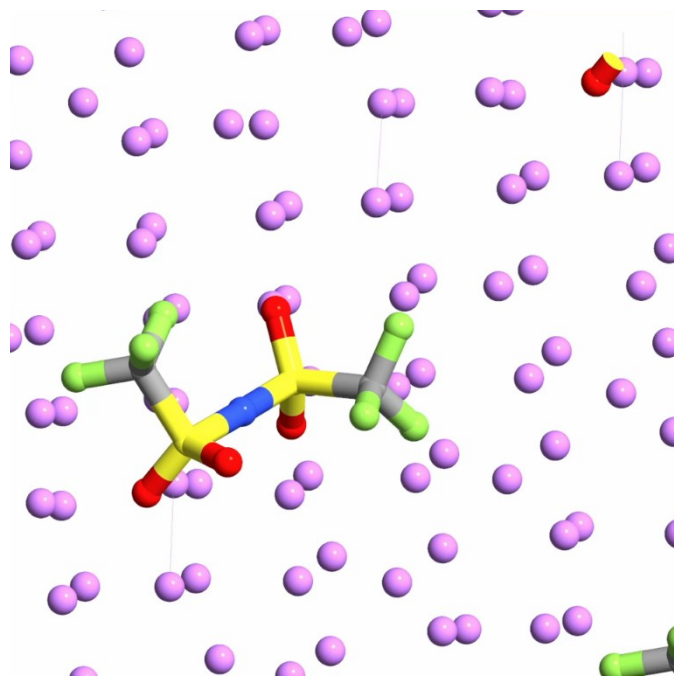



**Figure S7.** Bader charge evolutions correspond to the decomposed TMS molecule and the constituent atoms (S, O1, O2, and (CH<sub>2</sub>)<sub>4</sub>) in the LiTT system.



  
Video S2.mp4

**Video S2.** Molecular dynamic film of the decomposed TTE solvent in the LiTT electrolyte formulation.




  
Video S3.mp4

**Video S3.** Molecular dynamic film of the TFSI anion degradation process in contact with the Li anode surface in the LiTT electrolyte formulation.

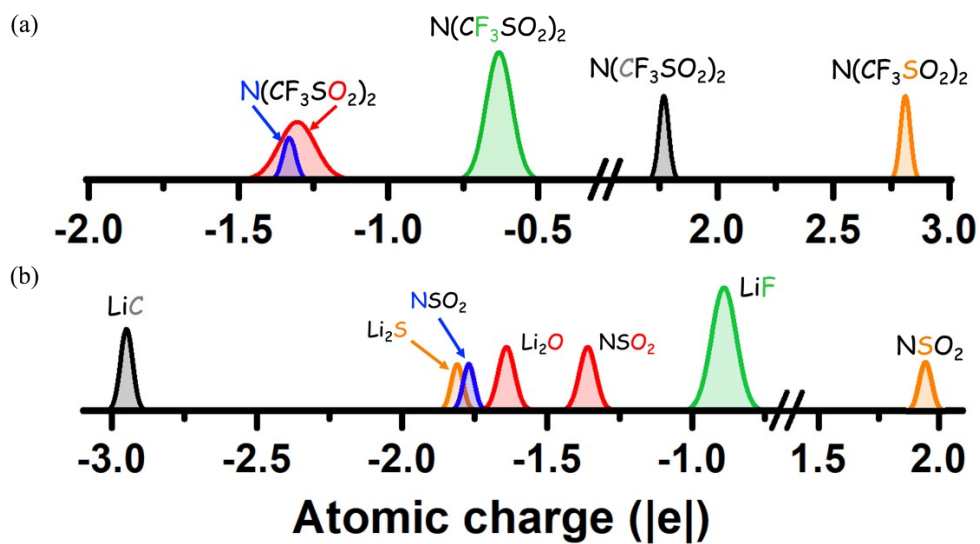
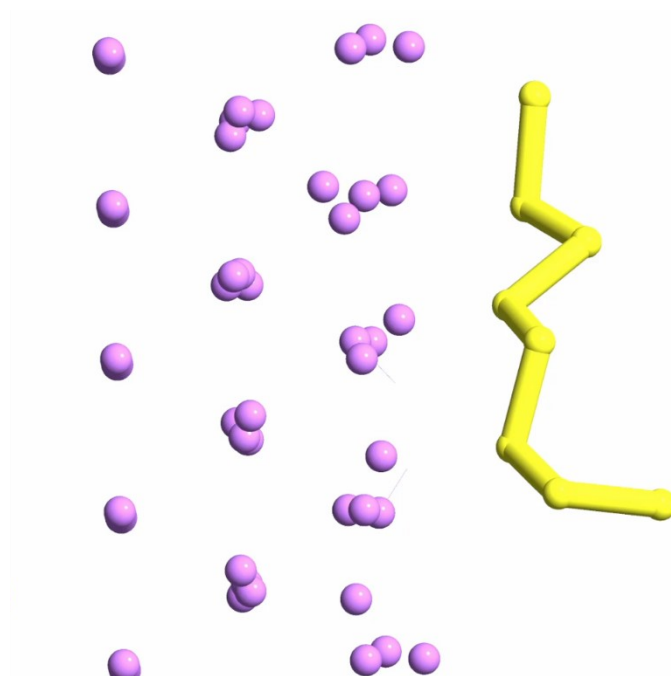


**Figure S8.** The atomic charge distributions of the constituent atoms from the reacted TFSI anion in the LiTT formulation at (a) 0 ps and (b) 15 ps of the simulated times. Color scheme: C, gray-black; S, orange; N, blue; O, red; F, green.



  
Video S4.mp4

**Video S4.** Molecular dynamic film of the PS additive degradation process in the LiTT-PS electrolyte formulation.

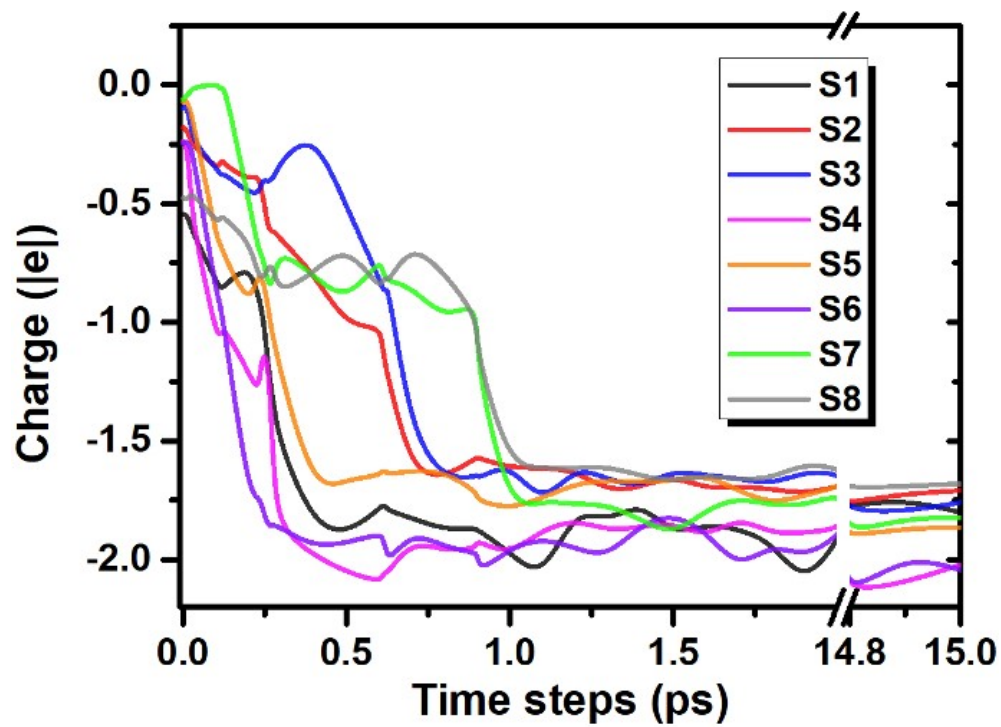


**Figure S9.** Bader charges evolutions of the constituent atoms (S1-S8) from the degraded PS additive in the LiTT-PS system.



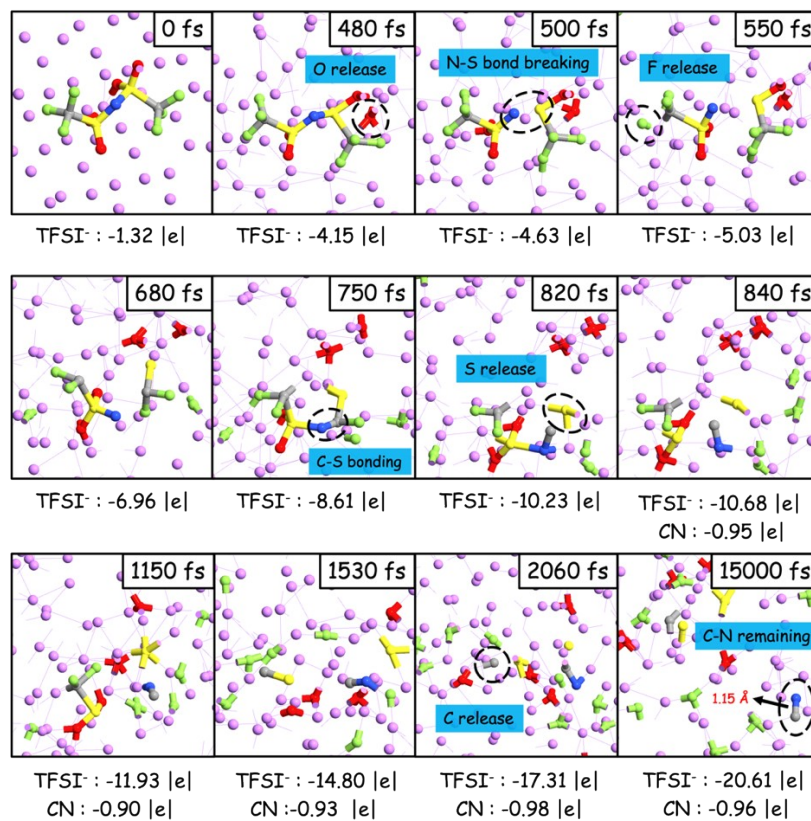


**Figure S10.** Extracted snapshots of the TFSI anion degradation process in contact with the Li anode surface in the LiTT-PS electrolyte formulation at different simulation time steps. Calculated Bader charges correspond to the TFSI anion, and the CN fragment is also shown at the bottom of each panel.

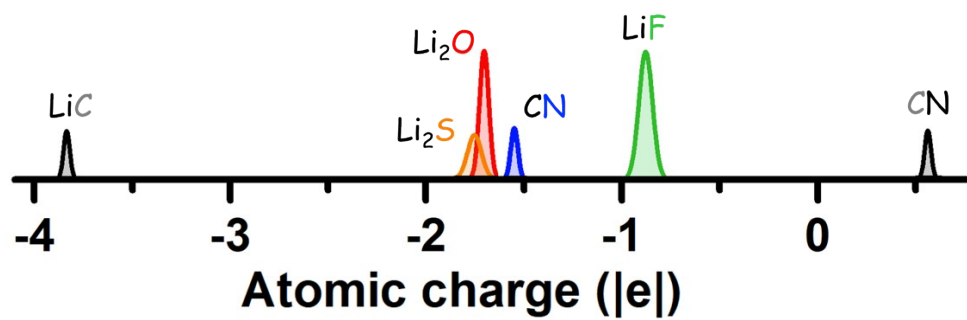


**Figure S11.** The atomic charge distributions of the constituent atoms from the reacted TFSI anion in the LiTT-PS formulation at the end of the simulated times.

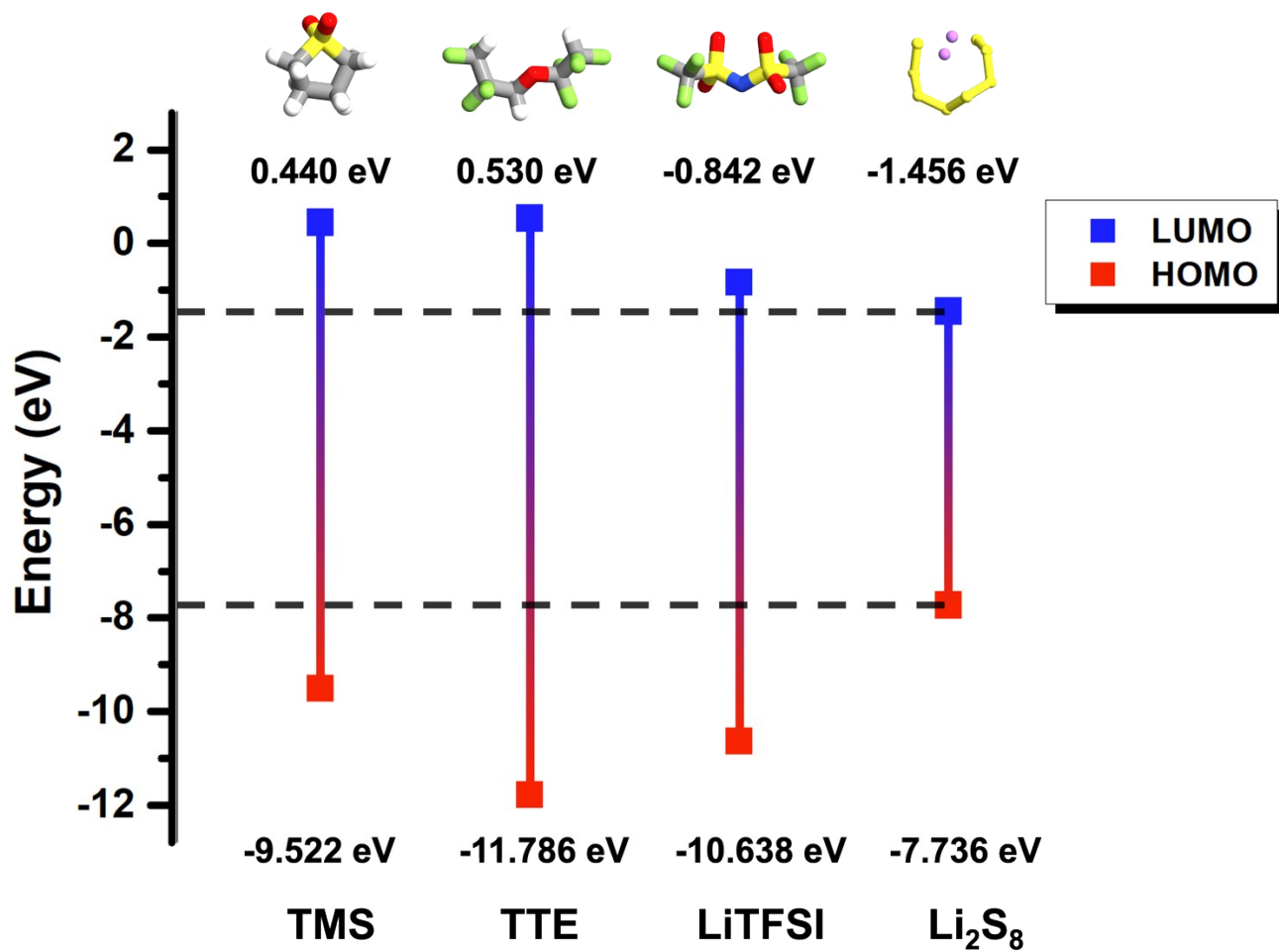
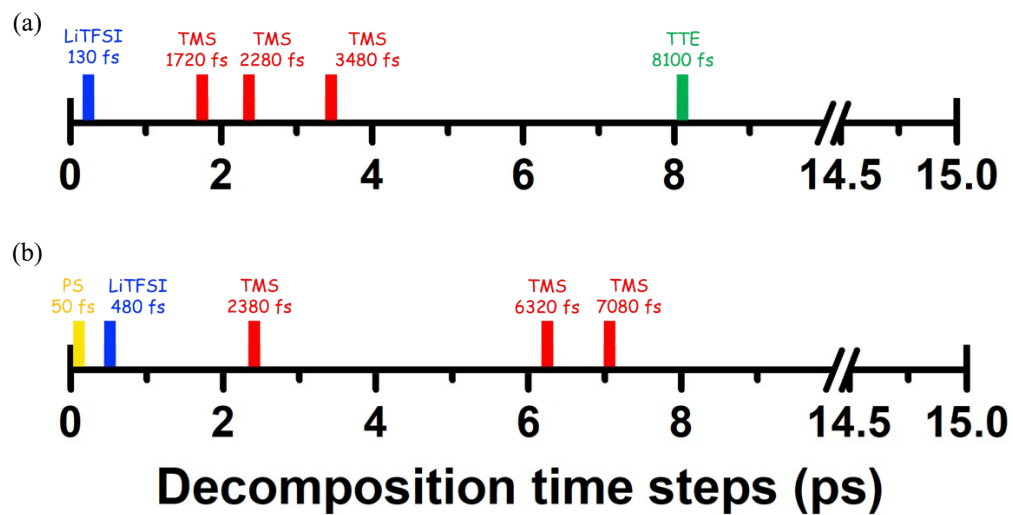


Figure S12. HOMO and LUMO energy levels of TMS, TTE solvents, LiTFSI salt, and Li<sub>2</sub>S<sub>8</sub> (PS) additive.



**Figure S13.** Reduction time steps of each electrolyte component in the (a) LiTT and (b) LiTT-PS formulations during the AIMD simulations.

**Table S2.** The calculated Bader charges of the constituent atoms from each SEI species in the LiTT and the LiTT-PS systems after the AIMD simulations (15ps).

	LiTT ( e )	LiTT-PS ( e )	SEI species
Li	0.034	0.057	Li <sup>0</sup>
	0.816	0.811	Li <sub>2</sub> O
	0.820	0.817	Li-C
	0.840	0.832	Li <sub>2</sub> S
	0.849	0.843	Li-N
	0.855	0.851	Li-F
S	-1.812	-1.843	Li <sub>2</sub> S
	<del>                    </del>	-0.240	S-S
	1.782	1.728	S-N
	2.501	2.404	S-C
	3.025	3.219	S=O
C	-2.941	-3.862	Li-C
	-0.012	-0.046	C-C/C-H
	0.140	0.135	C-S
	0.430	0.395	C-O
	1.727	1.706	C-F
O	-1.669	-1.658	Li-O-R
	-1.290	-1.292	C-O
	-1.018	-1.007	S=O
F	-0.912	-0.897	LiF
	-0.636	-0.629	CF <sub>2</sub>
	-0.631	-0.625	CF <sub>3</sub>
N	-1.776	-1.579	Li-N
	-1.263	-1.342	N-S

**Table S3** Fitting results of XPS analysis of Li foil after 24-h immersion tests.

	TMS	TMS-PS	TTE	TTE-PS	LiTT	LiTT-PS	Assignment/Ref.
Li 1s	52.2 eV, 23.1% 53.3 eV, 40.1% 54.4 eV, 28.1% 55.1 eV, 8.7%	52.3 eV, 17.7% 53.3 eV, 24.4% 54.4 eV, 35.4% 55.1 eV, 22.4%	52.1 eV, 24.2% 53.3 eV, 36.5% 54.3 eV, 30.5%  55.6 eV, 8.9%	52.1 eV, 38.0% 53.3 eV, 30.7% 54.3 eV, 10.1% 54.9 eV, 10.2%  55.8 eV, 11.0%	51.8 eV, 25.8% 53.2 eV, 13.2% 54.6 eV, 7.8 % 55.9 eV, 9.4 % 56.8 eV, 14.4% 57.9 eV, 29.8%	51.7 eV, 19.1% 53.1 eV, 20.6% 54.5 e, 30.3% 55.7 eV, 12.2% 56.8 eV, 6.3% 57.9 eV, 11.5%	Li <sup>0</sup> (52.3 eV) <sup>15</sup> Li <sub>2</sub> O (53.7 eV) <sup>15</sup> Li-C (55.5 eV) <sup>15</sup> Li <sub>2</sub> S (54.4 eV) <sup>16</sup> Li-N (55.5 eV) <sup>17</sup> Li-F (56.8 eV) <sup>18</sup>
S 2p	161.3 eV, 9.1%  165.7 eV, 53.8% 167.7 eV, 37.1%	161.3 eV, 8.6 % 164.4 eV, 15.5%  166.5 eV, 23.4% 167.8 eV, 52.5%,	NA	161.3 eV, 47.8% 164.5 eV, 52.2%	162.5 eV, 10.6%  164.8 eV, 9.6% 166.7 eV, 15.3% 168.9 eV, 64.6%	162.4 eV, 5.7% 164.3 eV, 15.9% 164.8 eV, 11.1% 166.7 eV, 21.2% 168.9 eV, 52.8%	Li <sub>2</sub> S (161.3eV) <sup>19</sup> S-S (164.1 eV) <sup>20</sup> S-N (163.7 eV) <sup>21</sup> S-C (164.6 eV) <sup>19</sup> S=O (168.2eV) <sup>20</sup>
C 1s	282.1 eV, 52.6%  284.0 eV, 30.7% 285.7 eV, 16.8%	282.0 eV, 70.2%  284.1 eV, 15.0% 285.8 eV, 14.8%	281.8 eV, 48.3%, 283.5 eV, 17.1%, 284.0 eV, 32.3%  285.4 eV, 6.7%, 287.4 eV, 5.0%	281.8 eV, 79.1% 283.6 eV, 7.5% 284.0 eV, 5.8%  285.8 eV, 5.3%, 287.3 eV, 2.3%,	281.7 eV, 39.5%  282.8 eV, 19.4% 284.9 eV, 8.0% 286.4 eV, 16.0% 287.7 eV, 17.5%	281.9 eV, 6.1%  282.9 eV, 48.0% 284.9 eV, 27.0% 286.2 eV, 10.3% 287.8 eV, 8.5%	Li-C (282.4 eV) <sup>15</sup> C=C (~284 eV) <sup>22</sup> C-C/C-H (284.4/285.5 eV) <sup>22, 23</sup> C-S (285.2 eV) <sup>19</sup> C-O (285.7 eV) <sup>23</sup> C-F (288.5 eV) <sup>24</sup>
O 1s	529.0 eV, 40%  530.9 eV, 54.6%	529.1 eV, 34.9%  531.1 eV,65.1%	528.8 eV, 42.6% 530.5 eV, 57.4%	528.8 eV, 58.9% 530.5 eV,41.1%	526.4 eV, 43.7% 532.3 eV, 44.7% 528.8 eV, 11.6%	526.4 eV, 8.5% 532.9 eV, 27.0% 528.7 eV, 64.5%	Li-O-R (530.9, 528.7 eV) <sup>25,15</sup> C-O (530.5 eV) <sup>26</sup> S=O (531.2 eV) <sup>27</sup>
F 1s	NA	NA	NA	NA	686.1 eV, 63.4% 688.8 eV, 12.2% 690.6 eV, 24.3%	686.1 eV, 25.5% 688.9 eV, 43.7% 691.9 eV, 30.7%	LiF (686.3 eV) <sup>28</sup> CF <sub>2</sub> (688.5 eV) <sup>29</sup> CF <sub>3</sub> (689.5 eV) <sup>29</sup>
N 1s	NA	NA	NA	NA	400.9 eV, 56.4% 399.7 eV, 43.6%	401.0 eV, 65.8% 399.9 eV, 34.2%	Li-N (400.1 eV) <sup>30</sup> N-S (398.9 eV) <sup>31</sup>

NA: Not applicable

The results shown in Figure S14 indicate that LiTFSI decomposed over the Li surface. The difference spectra by subtracting the liquid FTIR spectrum of (TMS/TTE=1/1 equal volume mixture) from that of LiTT (LiTFSI-TTE/TMS) is shown in Figure S14 (a), wherein the bands of TFSI anion can be used as a reference to that over Li surface. The bands at 1354 ( $\nu_{as}$  O=S=O), 1196 ( $\nu_s$  O=S=O/ $\nu_{as}$  C-F), 1128 ( $\nu_s$  C-F), 1059 ( $\nu_{as}$  S-N-S), 792 ( $\nu$  C-S), 759 ( $\nu_s$  S-N-S) and 704  $\text{cm}^{-1}$  ( $\delta$  C-F) can be attributed to TFSI anion in liquid phase based on references<sup>5-7, 13</sup>. Figure S14 (b) is from our previous work of LiTFSI/DME-DOL over Li metal anode<sup>32</sup>, wherein DME and DOL solvents would not chemically react with Li metal while LiTFSI will. This DRIFTS difference spectrum of DME-DOL from that of LiTFSI/DME-DOL (Figure S14 (b)) over Li metal anode can reveal contributing bands of LiTFSI over Li metal. From this difference spectrum, the bands at 1348 ( $\nu_{as}$  O=S=O), 1196 ( $\nu_s$  O=S=O/ $\nu_{as}$  C-F), 1132 ( $\nu_s$  C-F), 1024 ( $\nu_{as}$  S-N), 768 ( $\nu_s$  S-N/ $\nu$  C-S) and 702  $\text{cm}^{-1}$  ( $\delta$  C-F) attributed to TFSI anion bands over Li metal. When DRIFTS spectra of TFSI anion (Figure S14 (b)) compared to liquid FTIR spectra (Figure S14 (a)), the band related to O=S=O and S-N-S red-shifted to low frequency, i.e.,  $\nu_{as}$  O=S=O shifted from 1354 to 1348,  $\nu_{as}$  S-N-S from 1059 to 1024 and  $\nu$  C-S from 792 to 768 $\text{cm}^{-1}$ . When compared to previous pure solid ATR-FTIR spectra of LiTFSI<sup>13</sup>,  $\nu_{as}$  O=S=O band red-shifted to low frequency (from 1357 to 1348  $\text{cm}^{-1}$ ) and  $\nu_{as}$  S-N red-shifted to low frequency (1062 to 1024  $\text{cm}^{-1}$ ). The red shift in frequency of TFSI anions bands over Li metal related to the charge transfer reaction of  $\text{Li}^+$  with TFSI anion leading to S-N-S bond breaking formation of  $\text{Li-SO}_2\text{CF}_3$  and  $\text{Li}_2\text{-NSO}_2\text{CF}_3$  species over li electrode in agreement to previous DFT modeling report<sup>33</sup>. The band related to O=S=O showed a slight frequency shift due to  $\text{Li}^+$  bonded to O=S=O without bond breaking, but the band associated with S-N-S showed a more significant frequency shift due to S-N-S bond broken forming  $\text{Li-SO}_2\text{CF}_3$  and  $\text{Li}_2\text{-NSO}_2\text{CF}_3$  species. This indicates that the TFSI anion reacts with li metal and forms  $\text{Li-SO}_2\text{CF}_3/\text{Li}_2\text{-NSO}_2\text{CF}_3$  species when TMS/TTE or DOL/DME solvents are used. The TMS/TTE reacts with lithium metal at OCV, whereas DME/DOL is relatively stable at OCV.

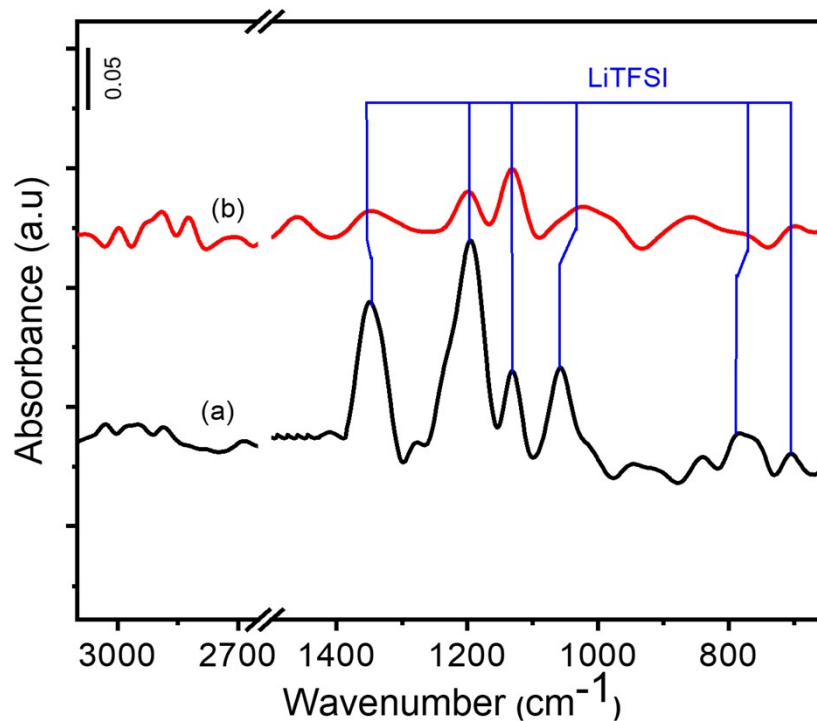


**Figure S14.** liquid FTIR difference spectra of TMS/TTE from spectra of (a) LiTT and DRIFTS difference spectra of (b) DME from DD-DOL.

In Figure S15, the difference spectra were done by subtracting the liquid FTIR spectra of each electrolyte component from corresponding DRIFTS spectra over the Li surface. The difference spectra provide bands nearly similar to its own DRIFTS spectra, indicating the surface species adsorbed over Li metal dominate in DRIFTS spectra more than that from the thin layer of liquid electrolyte component. This result confirms that decomposed species adsorbed over Li metal.



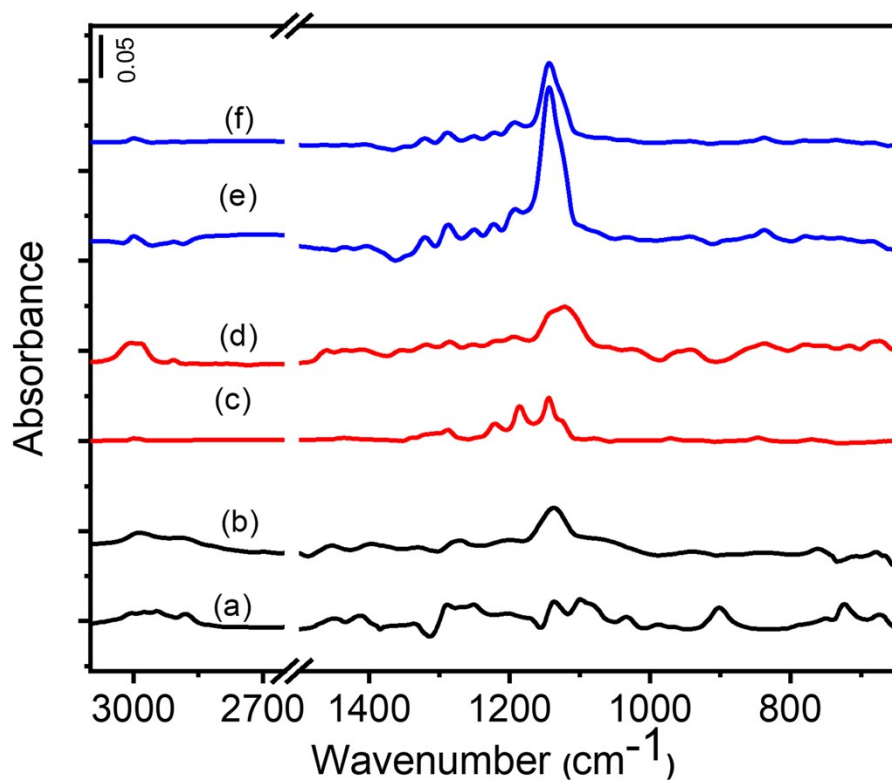


**Figure S15.** Difference spectrum of liquid FTIR of (a) TMS from DRIFTS of TMS, (b) TMS-PS from DRIFTS of TMS-PS, (c) TTE from DRIFTS of TTE, (d) TTE-PS from DRIFTS of TTE-PS, (e) LiTT from DRIFTS of LiTT and (f) LiTT-PS from DRIFTS of LiTT-PS over Li metal.

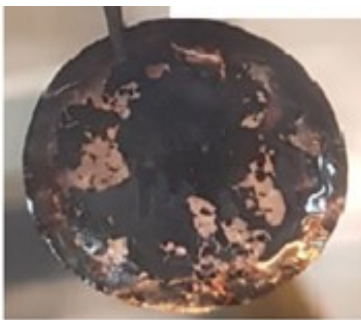


**Figure S16.** picture of copper electrode taken from Cu||Li cell after second lithiation cycle.

## Reference

1. J. Katon and W. Fearheller Jr, *Spectrochimica Acta*, 1965, **21**, 199-201.
2. H. M. Badawi, W. Förner, B. El Ali and A.-R. A. Al-Durais, *Spectrochimica Acta Part A: Molecular and Biomolecular Spectroscopy*, 2008, **70**, 983-990.
3. P. Basu, T. Ballinger and J. Yates Jr, *Langmuir*, 1989, **5**, 502-510.
4. L. Ng, J. Chen, P. Basu and J. Yates Jr, *Langmuir*, 1987, **3**, 1161-1167.
5. P. C. Howlett, N. Brack, A. F. Hollenkamp, M. Forsyth and D. R. Macfarlane, *Journal of the electrochemical society*, 2006, **153**, A595.
6. I. Rey, P. Johansson, J. Lindgren, J. Lassegues, J. Grondin and L. Servant, *The Journal of Physical Chemistry A*, 1998, **102**, 3249-3258.
7. J. Kiefer, J. Fries and A. Leipertz, *Applied spectroscopy*, 2007, **61**, 1306-1311.
8. R. L. Hudson, Y. Y. Yarnall and F. M. Coleman, *Spectrochimica Acta Part A: Molecular and Biomolecular Spectroscopy*, 2020, **233**, 118217.
9. D. S. Warren and A. J. McQuillan, *The Journal of Physical Chemistry B*, 2008, **112**, 10535-10543.
10. J. F. Vélez, M. Aparicio and J. Mosa, *The Journal of Physical Chemistry C*, 2016, **120**, 22852-22864.
11. S. Nunes, V. de Zea Bermudez, D. Ostrovskii, P. Barbosa, M. M. Silva and M. J. Smith, *Chemical Physics*, 2008, **345**, 32-40.
12. J.-C. Lassègues, J. Grondin, C. Aupetit and P. Johansson, *The Journal of Physical Chemistry A*, 2009, **113**, 305-314.
13. W. Kam, C.-W. Liew, J. Lim and S. Ramesh, *Ionics*, 2014, **20**, 665-674.
14. A. Nakanishi, K. Ueno, D. Watanabe, Y. Ugata, Y. Matsumae, J. Liu, M. L. Thomas, K. Dokko and M. Watanabe, *The Journal of Physical Chemistry C*, 2019, **123**, 14229-14238.
15. K. Kanamura, S. Shiraishi, H. Tamura and Z. i. Takehara, *Journal of The Electrochemical Society*, 1994, **141**, 2379.
16. Y. Gao, T. Rojas, K. Wang, S. Liu, D. Wang, T. Chen, H. Wang, A. T. Ngo and D. Wang, *Nature Energy*, 2020, **5**, 534-542.
17. C. Yan, Y. X. Yao, X. Chen, X. B. Cheng, X. Q. Zhang, J. Q. Huang and Q. Zhang, *Angewandte Chemie*, 2018, **130**, 14251-14255.
18. C.-u. Ro and R. W. Linton, *Surface Science Spectra*, 1992, **1**, 277-283.
19. A. A. Razzaq, Y. Yao, R. Shah, P. Qi, L. Miao, M. Chen, X. Zhao, Y. Peng and Z. Deng, *Energy Storage Materials*, 2019, **16**, 194-202.
20. Y. Li, K.-H. Wu, N. Huang, S. Dalapati, B.-J. Su, L.-Y. Jang, I. R. Gentle, D. Jiang and D.-W. Wang, *Energy Storage Materials*, 2018, **12**, 30-36.
21. N. Fechler, T.-P. Fellingner and M. Antonietti, *Journal of Materials Chemistry A*, 2013, **1**, 14097-14102.
22. L. Chen, Z. Xu, J. Li, B. Zhou, M. Shan, Y. Li, L. Liu, B. Li and J. Niu, *RSC Advances*, 2014, **4**, 1025-1031.
23. F. S. Reuter, C. J. Huang, Y. C. Hsieh, S. Dörfler, G. Brunklaus, H. Althues, M. Winter, S. D. Lin, B. J. Hwang and S. Kaskel, *Batteries & Supercaps*, 2021, **4**, 347-358.
24. I. V. Antonova, I. I. Kurkina, A. K. Gutakovskii, I. A. Kotin, A. I. Ivanov, N. A. Nebogatikova, R. A. Soots and S. A. Smagulova, *Materials & Design*, 2019, **164**, 107526.
25. S. Jiao, X. Ren, R. Cao, M. H. Engelhard, Y. Liu, D. Hu, D. Mei, J. Zheng, W. Zhao and Q. Li, *Nature Energy*, 2018, **3**, 739-746.
26. B. Shi, Y. Su, Y. Duan, S. Chen and W. Zuo, *Microchimica Acta*, 2019, **186**, 1-10.
27. L. Wilde, M. Polcik, J. Haase, B. Brena, D. Cocco, G. Comelli and G. Paolucci, *Surface science*, 1998, **405**, 215-227.
28. Y. He, Y. Zhang, P. Yu, F. Ding, X. Li, Z. Wang, Z. Lv, X. Wang, Z. Liu and X. Huang, *Journal of Energy Chemistry*, 2020, **45**, 1-6.
29. V. Shutthanandan, M. Nandasiri, J. Zheng, M. H. Engelhard, W. Xu, S. Thevuthasan and V. Murugesan, *Journal of Electron Spectroscopy and Related Phenomena*, 2019, **231**, 2-10.
30. C. Zha, X. Gu, D. Wu and H. Chen, *Journal of Materials Chemistry A*, 2019, **7**, 6431-6438.
31. J. Sharma, D. Downs, Z. Iqbal and F. Owens, *The Journal of Chemical Physics*, 1977, **67**, 3045-3049.
32. B. N. Olana, S. D. Lin and B.-J. Hwang, *Electrochimica Acta*, 2022, 140266.

33. L. E. Camacho-Forero, T. W. Smith, S. Bertolini and P. B. Balbuena, *The Journal of Physical Chemistry C*, 2015, **119**, 26828-26839.